PCCP

Accepted Manuscript

This is an *Accepted Manuscript*, which has been through the Royal Society of Chemistry peer review process and has been accepted for publication.

Accepted Manuscripts are published online shortly after acceptance, before technical editing, formatting and proof reading. Using this free service, authors can make their results available to the community, in citable form, before we publish the edited article. We will replace this *Accepted Manuscript* with the edited and formatted *Advance Article* as soon as it is available.

You can find more information about *Accepted Manuscripts* in the Information for Authors.

Please note that technical editing may introduce minor changes to the text and/or graphics, which may alter content. The journal's standard Terms & Conditions and the Ethical guidelines still apply. In no event shall the Royal Society of Chemistry be held responsible for any errors or omissions in this *Accepted Manuscript* or any consequences arising from the use of any information it contains.

ARTICLE

Gas Phase Selective Hydrogenation over Oxide Supported Ni-Au

Fernando Cárdenas-Lizana and Mark A. Keane*

5 The chemoselective continuous gas phase (*T* = 573 K; *P* = 1 atm) hydrogenation of nitroarenes (*p*-chloronitrobenzene (*p*-CNB) and *m*-dinitrobenzene (*m*-DNB)) has been investigated over a series of oxide (Al$_2$O$_3$ and TiO$_2$) supported Au and Ni-Au (1:10 mol ratio; 0.1-1 mol% Au) catalysts. Monometallic supported Au with mean particle size 3-9 nm promoted exclusive formation of *p*-chloroaniline (*p*-CAN) and *m*-nitroaniline (*m*-NAN). Selective hydrogenation rate was higher over smaller Au particles and can
10 be attributed to increased surface hydrogen (from TPD measurements) at higher metal dispersion. (S)TEM analysis has confirmed an equivalent metal particle size for the supported bimetallics at the same Au loading where TPR indicates Ni-Au interaction and EDX surface mapping established Ni in close proximity to Au on isolated nanoparticles with a composition (Au/Ni) close to the bulk value (=10). Increased spillover hydrogen due to the incorporation of Ni in the bimetallics resulted in elevated -NO$_2$
15 group reduction rate. Full selectivity to *p*-CAN was maintained over all the bimetallic catalysts. Conversion of *m*-DNB over the lower loaded Ni-Au/Al$_2$O$_3$ generated *m*-NAN as sole product. An increase in Ni content (0.01 →0.1 mol%) or a switch from Al$_2$O$_3$ to TiO$_2$ as support resulted in full –NO$_2$ reduction (to *m*-phenylenediamine). Our results demonstrate the viability of Ni-promotion of Au in the continuous production of functionalised anilines.

20 1. Introduction

The combination of two metallic elements has been shown to be an effective means of improving catalytic performance in a range of hydrogen mediated reactions, notably chemoselective hydrogenation (of nitro-compounds[1]), partial hydrogenation (of
25 alkynes[2]) and hydrogenolysis (of chlorophenols[3]). Renewed interest in Au as a catalytic agent has encompassed Au in bimetallic formulations, as noted in the recent review by Villa *et al.*[4] Gold has shown unique selectivity in the hydrogenation of polyfunctional reactants but delivers low reaction rates.[5] This
30 drawback has been ascribed to a restricted capacity for H$_2$ activation by dissociative chemisorption.[6] The combination of Au with transition metals that exhibit greater H$_2$ chemisorption capability offers a possible means of enhancing hydrogenation rate.
35 The hydrogenation response over bimetallic catalysts is determined by the structure and physico-chemical properties of the supported nanoparticles, which are dependent on the distribution of both metals within the crystal nanostructure. In order to achieve any degree of catalytic synergy, the two metals
40 must be in close proximity (if not in direct contact) on the support. The size, metal ratio and nature of the support are critical variables. Bimetallic particles at the nano-scale (~3 nm) can form solid solutions (homogeneous alloy particles) regardless of the miscibility gap between the two metallic elements.[7] The
45 incorporation of a second metal with Au (X-Au, where X = Pd,[8] Pt[9]) has been shown to increase hydrogenation activity but at low

Au/X ratios the selectivity response is affected or even governed by the second metal.[8, 9] The redox character and acid-base properties of the (oxide) carrier can act to stabilize small Au
50 nanoparticles as a result of electron transfer across the metal-support interface and induce geometric and electronic modifications that impact on catalysis.[5]

Prior research has focused on binary metals that form (ordered or random) bulk alloys with no miscibility gap in the
55 corresponding bulk phase diagram. This is the case with Pd-Au as the most widely studied Au-containing bimetallic.[10] Interest has shifted to systems such as Ni-Au that do not mix in the bulk but can form stable alloys in the outermost surface layers.[11, 12] The incorporation of Au onto partially oxidised Ni resulted in partial
60 oxidation of Au atoms and the formation of Au$_n$-O-Ni$_m$ ensembles (from XPS),[13] which were suggested as active sites in the isomerisation of methylstyrenes over Ni-Au/SiO$_2$.[14] Nishikawa *et al.*[15], studying the promotional effect of Au on Ni, demonstrated (by XRD, TEM, XAFS and [197]Au Mössbauer) the
65 formation of an Ni-Au alloy, following reduction (to 673 K in H$_2$) of Au/NiO co-precipitates. These were active in the hydrogenolysis of benzylic alcohols with superior catalytic activity compared with Raney Ni. Chin *et al.*[16] demonstrated by EXAFS/XANES analysis of Ni-Au/MgAl$_2$O$_4$ (prepared by
70 reductive deposition of Au on Ni/MgAl$_2$O$_4$) Au→Ni electron transfer with surface alloy formation that served to inhibit carbon deposition during *n*-butane steam reforming. The addition of Au to Ni (1:4) resulted in the formation of nano-crystals with a Au-core and Ni-enriched shell structure (based on EXAFS, XPS and
75 UV-vis) with increased hydrogenolysis activity in the conversion

of 2-phenoxy-1-phenylethanol.[17]

We have previously examined the catalytic action of supported Ni-Au with Ni/Au mol/mol = 10 in promoting gas phase nitroarene hydrogenation.[18, 19] That work was directed at the
[5] continuous selective production of industrially important functionalised amines under mild reactions conditions. Supported Ni-Au delivered higher hydrogenation activities but was less selective than supported Au. We have refocused our attention and have considered the possible role of Ni (introduced as the minor
[10] component; Ni/Au mol/mol = 0.1) to enhance the chemoselective hydrogenation action of Au to deliver enhanced rates to the target amine product. We assess the feasibility of controlling hydrogenation rate by varying Au particle size and the nature of the oxide support.

[15] ## 2. Experimental

2.1 Catalyst Preparation and Activation

The Al_2O_3 (Puralox, Condea Vista Co.) and TiO_2 (Degussa) supports were used as received. High (HL, 0.1 mol%) and low loaded (LL, 0.01 mol%) Ni/Al_2O_3 and/or Ni/TiO_2 catalyst
[20] precursors were synthesised by standard impregnation, where the support (6 g) was contacted with an aqueous $Ni(NO_3)_2$ solution (Aldrich, $7 \times 10^{-5} - 7 \times 10^{-4}$ M, 85 cm^3). The slurry was heated (2 K min^{-1}) to 353 K and maintained under constant agitation (600 rpm) in a He purge. The solid was dried in a flow of He at 383 K
[25] for 5 h and sieved (ATM fine test sieves) to mean particle diameter = 75 μm. The Au-Ni catalyst precursors were prepared by first reducing a batch of (LL and HL) Ni/Al_2O_3 and (LL) Ni/TiO_2 in a (60 cm^3 min^{-1}) H_2 stream at 2 K min^{-1} to 723 K, which was maintained for 1 h to ensure formation of zero valent
[30] Ni.[20] The gas flow was switched to He, cooled to ambient temperature and the samples passivated in 1% v/v O_2/He. This treatment served to provide a protective oxide layer over the surface Ni that prevented bulk oxidation upon exposure to the atmosphere. The passivated samples were treated with an
[35] aqueous $HAuCl_4$ solution (Aldrich, $3 \times 10^{-5} - 5 \times 10^{-4}$ M, 85 cm^3) to deliver a 10/1 Au/Ni mol ratio, post-treatment as above. Monometallic (HL, 1 mol% and LL, 0.1 mol %) Au/Al_2O_3 and (LL, 0.1 mol%) Au/TiO_2 were prepared by standard impregnation with aqueous $HAuCl_4$ (Aldrich, $7 \times 10^{-4} - 7 \times 10^{-3}$ M, 85 cm^3).
[40] Bulk metal loading was determined by ICP-OES (Vista-PRO, Varian Inc.).The Au-containing samples were stored under He in the dark at 277 K to avoid the deleterious effects of light (photodecomposition of cationic gold to Au^0)[21] and temperature (aggregation of Au precursor species).[22] Before reaction, the
[45] catalyst precursors were activated in 60 cm^3 min^{-1} H_2 at 2 K min^{-1} to 723 K (Ni/Al_2O_3 and Ni/TiO_2) or 603 K (Au/Al_2O_3, Au/TiO_2, $Ni-Au/Al_2O_3$, $Ni-Au/TiO_2$), which was maintained for 1 h.

2.2 Catalyst Characterisation

Specific surface area (SSA) and total pore volume measurements
[50] were made on a Micromeritics Flowsorb II 2300 unit. Prior to analysis, the samples were outgassed at 423 K for 1 h in 20 cm^3 min^{-1} N_2. SSA was obtained in a 30% v/v N_2/He flow (20 cm^3 min^{-1}) with at least three cycles of N_2 adsorption-desorption using the standard single-point BET method. Total pore volume was
[55] obtained at a relative N_2 pressure (P/P_0) = 0.95. The data were reproducible to ±3% and values quoted in this paper are the

mean.

Temperature programmed reduction (TPR), H_2 chemisorption and temperature programmed desorption (TPD) were determined
[60] using the CHEM-BET 3000 (Quantachrome) unit. The samples were loaded into a U-shaped Quartz cell (3.76 mm i.d.) and heated in 17 cm^3 min^{-1} 5% v/v H_2/N_2 (Brooks mass flow controlled) to 603 ± 1 K (Au/Al_2O_3, Au/TiO_2, $Ni-Au/Al_2O_3$ and $Ni-Au/TiO_2$) or 723 ± 1 K (Ni/Al_2O_3 and Ni/TiO_2) at 2 K min^{-1}.
[65] The effluent gas passed through a liquid N_2 trap and H_2 consumption was monitored by a thermal conductivity detector (TCD) with data acquisition/manipulation using the TPR Win™ software. The reduced samples were maintained at the final temperature in H_2 until return to baseline. After the reduction
[70] step, the samples were cooled in a He flow and subjected to H_2 chemisorption (at ambient temperature) using a pulse (10 μl) titration procedure, as described elsewhere.[23] TPD was conducted in a N_2 flow (65 cm^3 min^{-1}) at 50 K min^{-1} to 873 K with an isothermal hold until the signal returned to the baseline. The
[75] support alone was subjected to an equivalent TPR and subsequent TPD, which was used to correct for H_2 desorption from Al_2O_3.[24]

Metal particle morphology, size distribution and surface composition were determined by transmission electron microscopy using a JEOL JEM-2100F unit operating at an
[80] accelerating voltage of 200 kV with resolution to 0.14 nm and an EDAX Genesis XM 4 system 60. Samples were dispersed in 1-butanol by ultrasonic vibration, deposited on a lacey-carbon/Cu grid (200 Mesh) and dried at 383 K. Up to 300 individual metal particles were counted for each catalyst and the surface area-
[85] weighted metal diameter (d) was calculated from:

$$d = \frac{\sum_i n_i \cdot d_i^3}{\sum_i n_i \cdot d_i^2} \qquad (1)$$

where n_i is the number of particles of diameter d_i

2.3 Gas Phase Nitroarene Hydrogenation

2.3.1 Materials

[90] The reactants (p-chloronitrobenzene (p-CNB) and m-dinitrobenzene (m-DNB), Aldrich, ≥98%) and solvent (1-butanol, Riedel-de Haën, ≥99.5%) were used as supplied, without further purification.

2.3.2 Catalytic System

[95] Catalytic reactions were carried out under atmospheric pressure, in situ immediately after activation, in a fixed bed vertical continuous flow glass reactor (i.d. = 15 mm) at 573 K. The reactions were conducted under conditions of negligible heat/mass transport limitations. A preheating zone (layer of borosilicate glass beads)
[100] ensured that the nitroarene reactant was vaporised and reached reaction temperature before contacting the catalyst. Isothermal conditions (±1 K) were maintained by thoroughly mixing the catalyst with ground glass (75 μm) before insertion into the reactor. Temperature was continuously monitored by a thermocouple
[105] inserted in a thermowell within the catalyst bed. The p-CNB (or m-DNB) reactant was delivered, in a co-current flow of H_2, via a glass/teflon air-tight syringe and a teflon line, using a microprocessor controlled infusion pump (Model 100 kd Scientific) at a fixed calibrated flow rate, with an inlet -NO_2 molar flow (F_{-NO_2})

in the range $1.1 \times 10^{-4} – 3.1 \times 10^{-4}$ mol·h⁻¹, where the molar metal to inlet -NO$_2$ feed rate ratio spanned the range $1.1 \times 10^{-3} – 16.0 \times 10^{-3}$ h. The H$_2$ content was far in excess of the stoichiometric requirement for –NO$_2$ reduction (160-430), the flow rate of which was monitored using a Humonics (Model 520) digital flowmeter; $GHSV = 2 \times 10^4$ h⁻¹. In a series of blank tests, passage of p-CNB or m-DNB in a stream of H$_2$ through the empty reactor or over the supports alone did not result in any detectable conversion.

2.3.3 Analytical Method and Activity/Selectivity Evaluation

The reactor effluent was frozen in a liquid nitrogen trap for subsequent analysis using a Perkin-Elmer Auto System XL gas chromatograph equipped with a programmed split/splitless injector and a flame ionization detector, employing a DB-1 50 m × 0.20 mm i.d., 0.33 μm film thickness capillary column (J&W Scientific). Repeated catalytic runs with different samples from the same batch of catalyst delivered product compositions that were reproducible to within ±6% with a carbon balance of ±5%. Catalyst activity is quantified in terms of nitroarene (m-DNB ($X_{m\text{-DNB}}$) or p-CNB ($X_{p\text{-CNB}}$)) fractional conversion

$$X_{\text{nitroarene}} = \frac{[\text{nitroarene}]_{\text{in}} - [\text{nitroarene}]_{\text{out}}}{[\text{nitroarene}]_{\text{in}}} \quad (2)$$

where the subscripts "in" and "out" refer to inlet and outlet streams, respectively. Selectivity in terms of (*e.g.*) m-phenylenediamine (m-PDM) from m-DNB ($S_{m\text{-PDM}}$) is given by

$$S_{m\text{-PDM}} = \frac{[m\text{-PDM}]_{\text{out}}}{[m\text{-DNB}]_{\text{in}} - [m\text{-DNB}]_{\text{out}}} \times 100 \quad (3)$$

3. Results and Discussion

3.1 Catalyst Characterisation

The metal content, specific surface area (SSA), pore volume, H$_2$ uptake/release during TPR/TPD and mean metal particle size for the (mono- and bi-metallic) catalysts used in this study are given in **Table 1**. The SSA and pore volume of the Al$_2$O$_3$ support (191 m²·g⁻¹; 450×10^{-3} cm³·g⁻¹) are close to values reported for commercial Puralox mesoporous γ-Al$_2$O$_3$ (157 m²·g⁻¹; 420×10^{-3} cm³·g⁻¹).[25] Incorporation of Au and Ni resulted in a measurable decrease in SSA and pore volume that can be ascribed to partial pore filling by the metal(s) or Al$_2$O$_3$ dissolution during impregnation resulting in pore collapse.[26] The TiO$_2$ supported systems exhibited similar SSA and pore volumes to the starting support (52 m²·g⁻¹; 120×10^{-3} cm³·g⁻¹) that are in accord with Degussa P25 (61 m²·g⁻¹; 120×10^{-3} cm³·g⁻¹).[27]

The TPR profiles generated for Au/Al$_2$O$_3$-HL **(I)**, Au/Al$_2$O$_3$-LL **(II)** and Au/TiO$_2$-LL **(III)** can be compared in **Figure 1**.
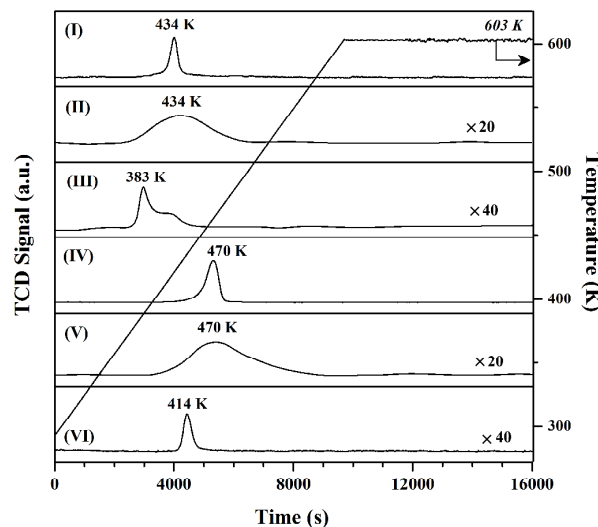
Fig. 1 TPR profiles generated for: **(I)** Au/Al$_2$O$_3$-HL, **(II)** Au/Al$_2$O$_3$-LL, **(III)** Au/TiO$_2$-LL, **(IV)** (1:10) Ni-Au/Al$_2$O$_3$-HL, **(V)** (1:10) Ni-Au/Al$_2$O$_3$-LL and **(VI)** (1:10) Ni-Au/TiO$_2$-LL.

The three samples present a principal H$_2$ consumption peak with an associated temperature maximum (T_{max}) over 383-434 K, which is within the range recorded elsewhere (328-465 K) for the activation of Au/Al$_2$O$_3$ and Au/TiO$_2$ and attributed to precursor reduction.[28] The lower T_{max} recorded for Au/TiO$_2$-LL (relative to Au/Al$_2$O$_3$) is consistent with the literature.[29] Moreover, Delannoy *et al.*[30] have demonstrated (by *in situ* XAFS and DRIFTS) greater reducibility of cationic gold on TiO$_2$ compared with Al$_2$O$_3$. Hydrogen consumption during catalyst activation was close to that required for Au³⁺ reduction (**Table 1**). Supported bimetallic catalyst preparation involved reductive deposition where Ni with a lower electrochemical potential (ECP = -0.27) acts to reduce the Au precursor (HAuCl$_4$, ECP = 1.00).[31] The TPR profiles generated for Al$_2$O$_3$ and TiO$_2$ supported Ni (not shown) exhibited a single broad H$_2$ consumption peak at the final isothermal hold (723 K) that can be associated with a combined decomposition-reduction of the precursor to metallic nickel, as noted elsewhere.[1] A single stage reduction was observed for the

Table 1 Physico-chemical characteristics of Al$_2$O$_3$ and TiO$_2$ supported mono- (Au) and bi-metallic (Ni-Au) catalysts.

Catalyst[a]	SSA[b] (m²·g⁻¹)	Pore Volume × 10⁻³[c] (cm³·g⁻¹)	TPR T_{max} (K)	TPR H$_2$ (μmol·g$_{catalyst}$⁻¹)[d,e]	H$_2$ TPD (mmol·mol$_{Au}$⁻¹)	d[f] (nm)
Au/Al$_2$O$_3$-HL	161	427	434	102[d] / 104[e]	473	9
Ni-Au/Al$_2$O$_3$-HL	189	444	470	151[d] / 145[e]	3118	9
Au/Al$_2$O$_3$-LL	169	425	434	9[d] / 16[e]	1101	4
Ni-Au/Al$_2$O$_3$-LL	190	447	470	9[d] / 8[e]	2471	4
Au/TiO$_2$-LL	49	117	383	11[d] / 15[e]	1233	3
Ni-Au/TiO$_2$-LL	47	115	414	12[d] / 15[e]	1765	3

[a] Au metal content (mol%): LL = 0.1, HL = 1.0, 1:10 Ni:Au molar ratio in bi-metallics; [b] Specific Surface Area (SSA), Al$_2$O$_3$ = 191 m²·g⁻¹, TiO$_2$ = 52 m²·g⁻¹; [c] Pore Volume, Al$_2$O$_3$ = 450 × 10⁻³ cm³·g⁻¹, TiO$_2$ = 120 × 10⁻³ cm³·g⁻¹; [d] H$_2$ required for the reduction of the metal precursor; [e] experimentally determined H$_2$ consumption; [f] surface area weighted mean metal particle size from TEM/STEM analysis.

ARTICLE

supported Ni-Au systems at a higher T_{max} (414-470 K) than that recorded for the corresponding monometallic Au catalysts. Modification to the TPR response for Au containing bimetallic catalysts with respect to monometallic counterparts has been reported and linked to interaction between both metals.[32] Pu *et al.*[33] have recently described a stabilisation of Au species (on activated carbon spheres) with the introduction of Ni by co-impregnation that inhibited reduction, displacing the temperature for $Au^{III} \rightarrow Au^0$ (from 583 K to 588 K) and $Au^I \rightarrow Au^0$ (from 619 K to 659 K) to higher values.

Gold particle size, from TEM analysis (**Figures 2** and **3** and **Table 1**), is dependent on metal loading and the nature of the support. The particle size in Au/Al_2O_3-HL was in the range 1-20 nm (**Figure 3(I)**) with a surface area weighted mean diameter of 9 nm. The lower Au loaded sample (Au/Al_2O_3-LL) exhibited a narrower size distribution (1-8 nm, **Figure 3(II)**) and smaller mean (4 nm). This effect is consistent with literature that has shown wider size range and the formation of larger nanoparticles with increasing Au content.[34] This can be linked to mobility of the chloride precursor, resulting in Au agglomeration during thermal treatment.[35] Enhanced Au dispersion on TiO_2 (**Figure 3(III)**) is a consequence of a difference in metal/support interaction relative to Au/Al_2O_3.[36] Loss of lattice oxygen with the formation of surface vacancies is a feature of thermal treatment in H_2 for reducible oxides such as TiO_2 at $T \geq 573$ K.[37] These surface defects act as Au nucleation sites with electronic interactions that limit particle growth, leading to enhanced dispersion.[38, 39]

Representative (S)TEM images of Ni-Au/Al_2O_3-HL **(I)**, Ni-Au/Al_2O_3-LL **(III)** and Ni-Au/TiO_2-LL **(IV)** can be compared in **Figure 4**. The metal size range in Ni-Au/Al_2O_3-HL (1-20 nm) coincided with Au/Al_2O_3-HL and there was no obvious alteration due the inclusion of Ni. This response extended to Ni-Au/Al_2O_3-LL and Ni-Au/TiO_2-LL with an equivalent mean metal size relative to the monometallic system (see **Table 1**). This can be attributed to the low Ni content in the bimetallic samples. An unchanged metal particle size has been reported previously for TiO_2 supported Au and Pt-Au with low Pt content (0.01-0.03% wt.).[9] EDX mapping (see representative analysis for Ni-Au/Al_2O_3-HL in **Figure 4(II)**) demonstrated that individual particles contained both Au and Ni in proportions close to the bulk value (Au/Ni = 10). EDX analysis cannot establish unequivocally the exact nature of Ni-Au interaction or rule out the occurrence of bimetallic clusters[40] or surface alloy.[41] Both possibilities have been suggested for Ni-Au catalysts prepared in an analogous manner and with a similar metal dispersion to that in this study. [16, 42, 43] Deghedi and co-workers[42] proposed the formation of Ni particles covered with Au adatoms (on the basis of EXAFS and TEM-EDX measurements) for Ni-Au/SiO_2 synthesised by redox deposition that contained metal ensembles of 5.1 nm. Maniecki and co-workers[44] reported an alloy phase (on the basis of XRD) for Ni-Au/Al_2O_3 prepared by co-impregnation (with $Ni(NO_3)_2$ and $HAuCl_4$) and reduction in H_2. Surface alloy
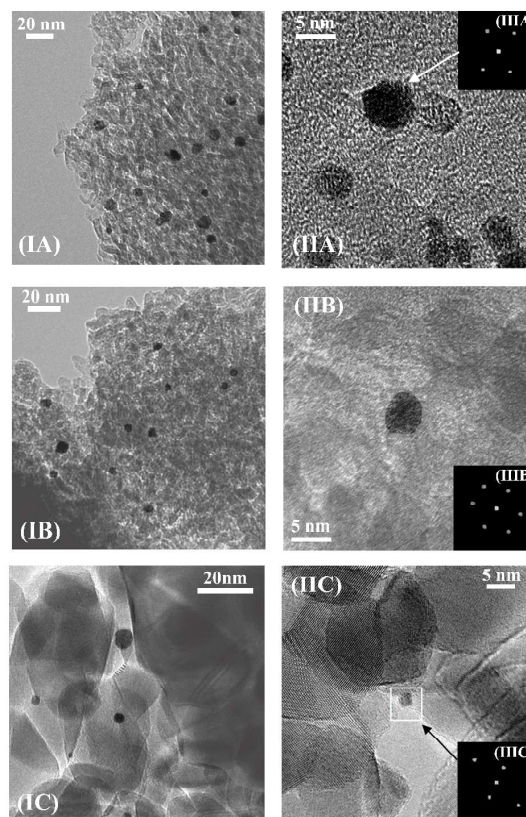

Fig. 2 Representative **(I)** medium and **(II)** high resolution TEM images with **(III)** associated diffractogram pattern of an isolated single Au nanoparticle in **(A)** Au/Al_2O_3-HL, **(B)** Au/Al_2O_3-LL and **(C)** Au/TiO_2-LL.
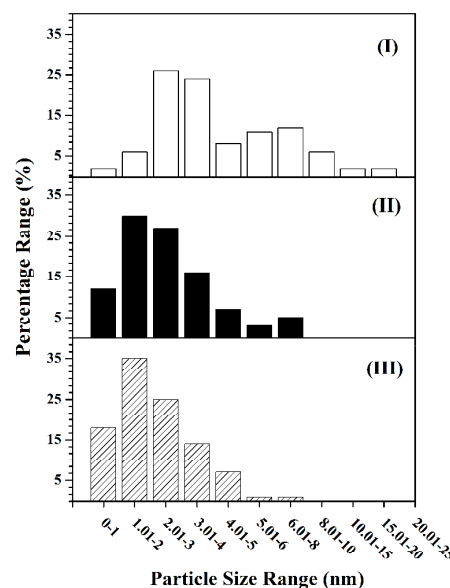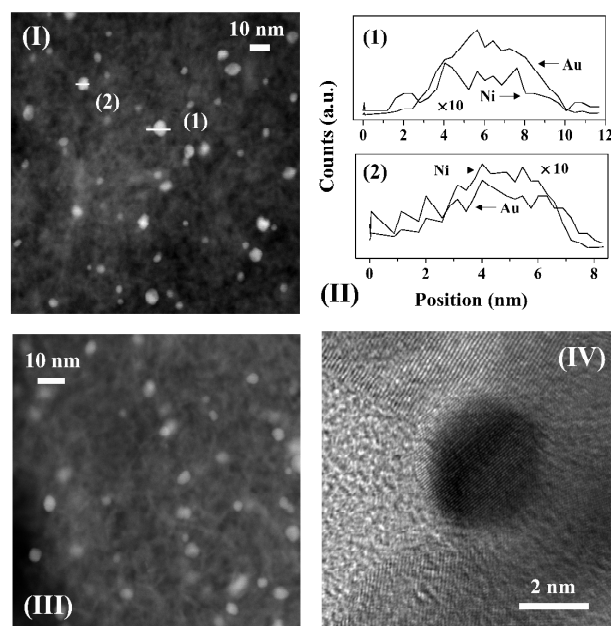

Fig. 3 Gold particle size distributions associated with **(I)** Au/Al_2O_3-HL (open bars), **(II)** Au/Al_2O_3-LL (solid bars) and **(III)** Au/TiO_2-LL (hatched bars).
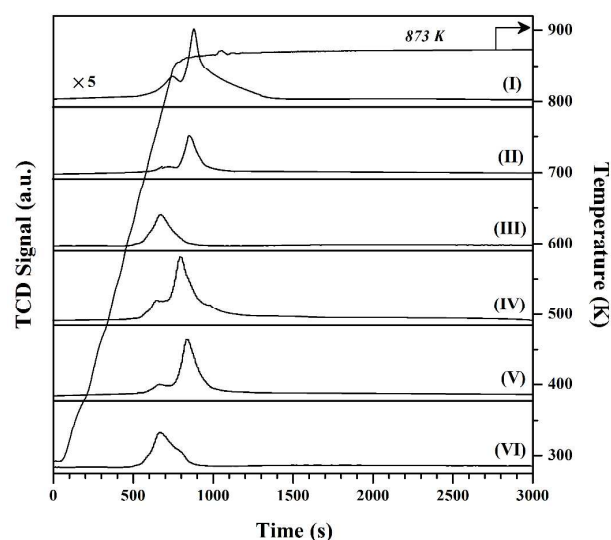
ARTICLE

Fig. 4 Representative TEM/STEM images of **(I)** Ni-Au/Al$_2$O$_3$-HL showing **(1)** 12 nm and **(2)** 8 nm segments across individual metal particles subjected to **(II)** EDX mapping with the associated Ni (counts × 10) and Au distribution, **(III)** Ni-Au/Al$_2$O$_3$-LL and **(IV)** Ni-Au/TiO$_2$-LL.

Fig. 5 Hydrogen TPD profiles generated for: **(I)** Au/Al$_2$O$_3$-HL, **(II)** Au/Al$_2$O$_3$-LL, **(III)** Au/TiO$_2$-LL, **(IV)** (1:10) Ni-Au/Al$_2$O$_3$-HL, **(V)** (1:10) Ni-Au/Al$_2$O$_3$-LL and **(VI)** (1:10) Ni-Au/TiO$_2$-LL.

formation was suggested by EXAFS/XANES for Au-Ni/MgAlO$_4$ (10.1 nm) prepared by redox deposition.[16] Molenbroek and Nørskov[43] also demonstrated the occurrence of a surface alloy in Ni-Au/SiO$_2$ (2.5-6.0 nm) and Ni-Au/MgAl$_2$O$_4$ (3.0-15.0 nm) by Monte Carlo simulations, which was experimentally verified by EXAFS, TEM and in-situ XRD.

The hydrogenation of nitroarenes is enhanced by contributions due to spillover hydrogen.[19, 36] The generation of spillover species involves dissociative adsorption of H$_2$ on a (*donor*) supported metal site with migration of the atomic hydrogen generated to the (*acceptor*) support.[45] Hydrogen TPD is a practical approach that can serve to quantify the degree of spillover. Ambient temperature H$_2$ chemisorption following TPR on all the catalysts was low ($\leq$15 mmol·mol$_{Au}^{-1}$) and close to the detection limits. Low uptake on supported Au has been demonstrated elsewhere and attributed to the filled *d*-band and high activation energy barrier for dissociative adsorption.[6, 46] There was no measurable difference in ambient temperature H$_2$ uptake on the bimetallics, which may be due to the low Ni content. The H$_2$ TPD profiles are presented in **Figure 5**. In all cases, the profiles show H$_2$ release with maxima at $T \geq 770$ K where the total amount desorbed (per mol$_{Au}$, **Table 1**) was appreciably greater (by two orders of magnitude) than that taken up in the chemisorption step. This response suggests the release of spillover hydrogen generated during catalyst activation by TPR.[45] The shift in the TPD peak for TiO$_2$ systems to a lower temperature (by up to a 100 K) is indicative of a less energetically demanding desorption of H$_2$.

This is consistent with literature[47, 48] that has reported a down-shift (by *ca.* 60-70 K) in the H$_2$-TPD peak for Ni/TiO$_2$ and Pd-Au/Al$_2$O$_3$-TiO$_2$ compared with Ni/Al$_2$O$_3$ and Pd-Au/Al$_2$O$_3$, respectively. Taking the three monometallic Au catalysts presented in **Figure 5**, H$_2$ desorbed (**Table 1**) increased in the order: Au/Al$_2$O$_3$-HL **(I)** < Au/Al$_2$O$_3$-LL **(II)** < Au/TiO$_2$-LL **(III)** where the values obtained are close (54-932 mmol·mol$_{Au}^{-1}$) to those reported elsewhere for Au with similar metal size (3-5 nm) supported on Fe$_2$O$_3$.[36] This sequence reflects that of decreasing mean Au nanoparticle size (**Table 1**). There is evidence in the literature[23] that metal size is a crucial variable controlling spillover where a greater (*donor*) surface area for smaller metal nanoparticles extends the *donor/acceptor* interface and facilitates spillover transfer. The profiles generated for the bimetallic Ni-Au catalysts (**Figure 5**, profiles **IV-VI**) reveals a significant increase in H$_2$ desorbed relative to Au samples with the same loading (see **Table 1**). This suggests a surface Ni/Au synergism that impacts on H$_2$ adsorption/desorption dynamics. The existing literature on Au containing bimetallics for hydrogenation applications has been from the perspective of Au as a diluent with low H$_2$ uptake capacity and a resultant decrease in surface hydrogen associated with the bimetallic.[49] As a result, there is no directly comparable H$_2$ TPD analysis for supported bimetallic Au-containing systems where the second metal was present in small amounts. We should flag the work of Wojcieszak *et al.*[50] who observed an increase in H$_2$ released (0.22 → 0.38 mol·g^{-1}) during TPD of Ni-Ag/SiO$_2$ with increasing Ni content (0.50→0.75 %wt.). It is important to note that Ni-Au/Al$_2$O$_3$-HL with lower metal dispersion showed significantly greater H$_2$ desorption (**Table 1**) relative to Ni-Au/Al$_2$O$_3$-LL. STEM-EDX analyses have demonstrated the presence of both metals on individual nanoparticles. The formation of bimetallic nano-crystals (*i.e.* Au decorating Ni

nanoparticles) has been demonstrated (EXAFS and TEM-EDS) for Ni-Au bimetallics prepared and activated using a similar methodology.[42] It is known that H_2 interaction is distinct for monometallic, bimetallic and alloy nanoparticles.[51, 52] The greater Ni loading in Ni-Au/Al_2O_3-HL (0.1 mol% vs. 0.01 mol%) must facilitate H_2 dissociative adsorption and spillover during TPR, which is reflected in greater H_2 release during TPD. In the case of the low loading bimetallics, H_2 desorption from Ni-Au/Al_2O_3-LL exceeded Ni-Au/TiO_2-LL (**Table 1**). This can be tentatively linked to modifications induced by the support that impact on H_2 uptake on the bimetallic phase. Likewise, Gu et al.[47] observed an greater H_2 TPD from Pd-Au/Al_2O_3 relative to Pd-Au/Al_2O_3-TiO_2. The characterisation analysis has established the formation of nano-scale (mean=3-9 nm) Au particles in the monometallics with greater surface hydrogen for catalysts with increasing metal dispersion. TPR measurements suggest interaction of Ni with Au in the bimetallics. STEM-EDX analysis has demonstrated the presence of Au and Ni in individual nanoparticles and the TPD results are consistent with increased spillover resulting from Au/Ni synergy that increases the available surface hydrogen.

### 3.2 Gas Phase Nitroarene Hydrogenation

The hydrogenation of p-CNB and m-DNB over all the catalysts delivered time-invariant conversions (not shown) and exclusive nitro-group reduction with no evidence of hydrodechlorination, hydrodenitrogenation or aromatic ring reduction. This combined stability/selectivity is important in terms of the viable application of Au catalyst formulations in the production of functionalised anilines. Catalyst deactivation in hydrogenation (of naphthalene,[53] 1,3-butadiene[54] and acetylene[55, 56]) has been reported for Au supported on Al_2O_3[53, 54, 57] and TiO_2[55, 56] and ascribed to metal sintering[54, 55] and coking.[55-57] Moreover, temporal loss of activity in the gas phase hydrogenation of nitroarenes over Pd/Al_2O_3 has been observed and linked to coke formation.[58, 59]

Table 2 Catalysis results: pseudo-first order rate constant (k) and product distribution (at $X \sim 0.07$) in the hydrogenation of p-CNB and m-DNB over Al_2O_3 and TiO_2 supported monometallic (Au) and bimetallic (Ni-Au; 1:10 molar ratio) catalysts; Reaction conditions: P = 1 atm, T = 573 K.

Catalyst	p-CNB		m-DNB	
	k^a	Product(s) ($S_{product}$, %)	k^a	Product(s) ($S_{product}$, %)
Au/Al_2O_3-HL	4	p-CAN (100)	6	m-NAN (100)
Ni-Au/Al_2O_3-HL	24	p-CAN (100)	40	m-NAN (60) m-PDM (40)
Au/Al_2O_3-LL	12	p-CAN (100)	16	m-NAN (100)
Ni-Au/Al_2O_3-LL	21	p-CAN (100)	35	m-NAN (100)
Au/TiO_2-LL	18	p-CAN (100)	22	m-NAN (100)
Ni-Au/TiO_2-LL	22	p-CAN (100)	25	m-NAN (80) m-PDM (20)

^{a}mol$_{-NO_2}$·mol$_{Au}^{-1}$·h^{-1}

The applicability of pseudo-first order kinetics for the gas phase hydrogenation of p-CNB[1, 60] and m-DNB[36] has been established elsewhere. The extracted specific (per mol$_{Au}$) pseudo-first order rate constants (k) are given in **Table 2**. The promoting effect of Ni is demonstrated by the significantly increased hydrogenation rate when compared with the monometallic Au catalysts with the same loading. Under the same reaction conditions, Ni/Al_2O_3 and Ni/TiO_2 delivered negligible activity. Duan and co-workers[61] using unsupported nano-crystals reported increased rate (mol$_{product}$·mol$_{metal}^{-1}$) in the high pressure (40 atm) liquid phase hydrogenation of phenol (283 → 363) and benzene (164 → 261) over Ni-Rh relative to Rh, which was attributed to the bimetallic character of the nanoparticles (based on HRTEM-EDX and XRD) and possible modifications in active site electron density. Lu et al.[62, 63] recorded higher activity in the liquid phase hydrogenation of a series of p-substituted nitro-derivates over Ni-Pd colloids, ascribed to the formation of a Ni enriched alloy (from XRD, EXAFS, XPS). The elevated rate observed in this study can be linked to surface available reactive hydrogen as shown in **Figure 6** where H_2-TPD is related to the rate constant. The increase in surface hydrogen that results from incorporation of Ni with Au was accompanied by a higher hydrogenation rate. Moreover, reaction of m-DNB uniformly generated greater rates, a result that can be attributed to the activating effect of the second –NO_2 group, which is consistent with a nucleophilic mechanism, as demonstrated previously.[64]
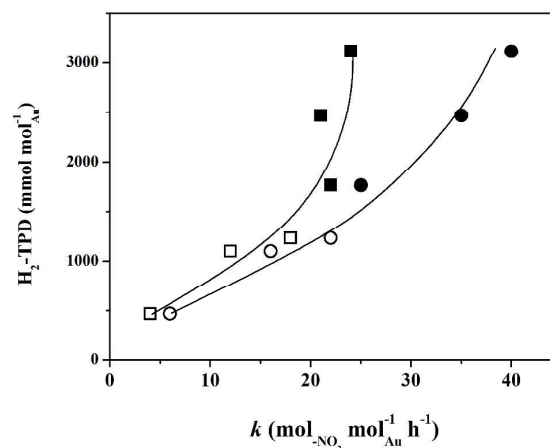
Fig. 6 Variation in hydrogen TPD (H_2-TPD) with pseudo-first order rate constant (k) in the hydrogenation of p-CNB (□, ■) and m-DNB (○, ●) over supported Au (open symbols) and Ni-Au (solid symbols) catalysts.

Reaction selectivity is compared at the same degree of conversion in **Table 2**. p-CNB was converted solely to the target (p-chloroaniline) p-CAN over all the catalysts, which is consistent with reaction exclusivity in continuous gas phase p-CNB→p-CAN over oxide supported Au.[49] In contrast, nitrobenzene,[1] aniline[1] and benzene[65] have been observed in the gas phase hydrogenation of CNB over Ru,[65] and Pd[1] catalysts. Variations in product distribution are, however, evident in the hydrogenation of m-DNB and sensitive to the nature of the catalyst. Full selectivity to partially reduced (m-nitroaniline) m-NAN was obtained over monometallic Au systems. In batch liquid phase operation, high pressures (26-34 atm) have been deemed essential to achieve high selectivity (84-98%) to m-

NAN.[48, 66] Preferential –NO2 activation on oxide supported Au in the presence of other reactive (C=C, carbonyl, amide and ester) functional groups has been demonstrated by FTIR analysis.[67] The incorporation of Ni at low loading (Ni-Au/Al2O3-LL) served to increase rate while retaining 100% selective to *m*-NAN. Deghedi *et al.*[42] reported that the combination of Au and Ni on SiO2 (Ni:Au molar ratio = 4:1) lowered the rate of C=C bond and aromatic ring hydrogenation relative to Ni in the conversion of styrene, which was accounted for in terms of geometric and electronic effects. At higher loadings (Ni-Au/Al2O3-HL) complete hydrogenation to *m*-PDM was observed, which is a characteristic of catalysis by Ni.[18, 19] This may be a consequence of increased surface reactive hydrogen which facilitates reduction of both –NO2 substituents. Alternatively, *m*-DNB activation on Ni-Au/Al2O3-HL may be distinct from Ni-Au/Al2O3-LL with a planar adsorption on the former through the aromatic ring, resulting in the formation of a resonance structure with two positive localised charges where both –NO2 groups are activated for nucleophilic attack. It is known that substituted aromatics interact with supported Ni catalysts *via* the π electron-delocalised aromatic ring.[68] Lonergan *et al.*[69] have observed *n*-butane selectivity effects in 1,3-butadiene hydrogenation over Ni-Pt/Al2O3 with increasing Ni content (1:3 → 1:10). The formation of *m*-PDM was also promoted over Ni-Au/TiO2-LL, which suggests a support effect in terms of *m*-DNB adsorption/activation that acts in tandem with differences in available reactive hydrogen. Wang *et al.*[70] reported a modified catalytic response in the hydrogenation of 1,3-budatiene for Pt-Ni on Al2O3 and TiO2. DFT calculations revealed stronger metal interaction with Al2O3 (binding energy *ca.* -50 kcal·mol^{-1}) than TiO2 (-17 kcal·mol^{-1}) with a preferential Ni-Al2O3 interaction at the metal-support interface leading to a Pt-terminated bimetallic configuration. A weaker Ni interaction in the case of the TiO2 carrier can then result in some segregation of the Ni component to the nanoparticle surface.

4. Conclusions

Oxide (Al2O3 and TiO2) supported Au (1 and 0.1 mol%) prepared by impregnation with subsequent activation generated nano-scale metal particles of mean size 3-9 nm. A decrease in Au size was accompanied by increased surface hydrogen (from TPD analysis) with higher specific chemoselective hydrogenation rate in the conversion of *p*-CNB → *p*-CAN and *m*-DNB → *m*-NAN. Supported bimetallic synthesis by reductive deposition of Au on Ni (where Au/Ni = 10) generated an equivalent particle size at the same Au loading but elevates the available surface hydrogen with a significant increase in –NO2 group reduction rate. TPR analysis suggests Ni-Au interaction where TEM-EDX mapping across isolated single particles has established Au and Ni in close proximity with a surface Au/Ni that coincided with the bulk value. Reaction of *p*-CNB over the bimetallics delivered full selectivity to *p*-CAN. Conversion of *m*-DNB was fully selective to *m*-NAN over monometallic Au and Ni-Au/Al2O3-LL. The hydrogenation of both –NO2 substituents (to *m*-PDM) was promoted over Ni-Au/Al2O3-HL and Ni-Au/TiO2-LL. This is attributed to the higher Ni loading that elevated the surface supply of hydrogen and possible electronic/geometric modifications induced by the support that impact on the *m*-DNB

adsorption/activation. We have demonstrated Au/Ni synergy that serves to enhance –NO2 reduction rate.

References

1. F. Cárdenas-Lizana, S. Gómez-Quero, C. Amorim and M. A. Keane, *Appl. Catal. A: Gen.*, 2014, **473**, 41.
2. A. Yarulin, I. Yuranov, F. Cárdenas-Lizana, D. T. L. Alexander and L. Kiwi-Minsker, *Appl. Catal. A: Gen.*, 2014, **478**, 186.
3. G. Yuan, C. Louis, L. Delannoy and M. A. Keane, *J. Catal.* , 2007, **247**, 256.
4. A. Villa, D. Wang, D. S. Su and L. Prati, *Catal. Sci. Technol.*, 2015, **5**, 55.
5. F. Cárdenas-Lizana and M. A. Keane, in *Gold Catalysis: Preparation, Characterization and Applications in the Gas and Liquid Phase*, eds. L. Prati and A. Villa, Pan Stanford Publishing, Singapore, 2014.
6. C. Kartusch and J. A. van Bokhoven, *Gold Bull.*, 2009, **42**, 343.
7. G. C. Bond, *Platinum Metals Rev.*, 2007, **51**, 63.
8. F. Cárdenas-Lizana, S. Gómez-Quero, A. Hugon, L. Delannoy, C. Louis and M. A. Keane, *J. Catal.*, 2009, **262**, 235.
9. D. P. He, X. D. Jiao, P. Jiang, J. Wang and B. Q. Xu, *Green Chem.*, 2012, **14**, 111.
10. C. Louis, in *Environmental Catalysis over Gold-based Materials*, eds. G. Avgouropoulos and T. Tabakova, The Royal Society of Chemistry, Cambridge, 2013.
11. F. Besenbacher, I. Chorkendorff, B. S. Clausen, B. Hammer, A. M. Molenbroek, J. K. Nørskov and I. Stensgaard, *Science*, 1998, **279**, 1913.
12. L. P. Nielsen, F. Besenbacher, I. Stensgaard, E. Laegsgaard, C. Engdahl, P. Stoltze, K. W. Jacobsen and J. K. Nørskov, *Phys. Rev. Lett.*, 1993, **71**, 754.
13. A. G. Rybkin, D. Y. Usachev, A. Y. Varykhalov, A. M. Shikin and V. K. Adamchuk, *Phys. Sol. State*, 2007, **49**, 984.
14. A. V. Naumkin and A. Y. Vasil'kov, *Russ. Chem. Bull.*, 2013, **62**, 2559.
15. H. Nishikawa, D. Kawamoto, Y. Yamamoto, T. Ishida, H. Ohashi, T. Akita, T. Honma, H. Oji, Y. Kobayashi, A. Hamasaki, T. Yokoyama and M. Tokunaga, *J. Catal.*, 2013, **307**, 254.
16. Y.-H. Chin, D. L. King, H.-S. Roh, Y. Wang and S. M. Heald, *J. Catal.*, 2006, **244**, 153.
17. J. Zhang, H. Asakura, J. van Rijn, J. Yang, P. Duchesne, B. Zhang, X. Chen, P. Zhang, M. Saeys and N. Yan, *Green Chem.*, 2014, **16**, 2432.
18. F. Cárdenas-Lizana, S. Gómez-Quero, G. Jacobs, Y. Ji, B. H. Davis, L. Kiwi-Minsker and M. A. Keane, *J. Phys. Chem. C*, 2012, **116**, 11166.
19. F. Cárdenas-Lizana, S. Gómez-Quero, C. J. Baddeley and M. A. Keane, *Appl. Catal. A: Gen.*, 2010, **387**, 155.
20. F. Cárdenas-Lizana, S. Gómez-Quero and M. A. Keane, *Appl. Catal. A: Gen.*, 2008, **334**, 199.
21. W.-S. Lee, B.-Z. Wan, C.-N. Kuo, W.-C. Lee and S. Cheng, *Catal.*

Commun., 2007, **8**, 1604.

22. R. Zanella and C. Louis, *Catal. Today*, 2005, **107-108**, 768.

23. C. Amorim and M. A. Keane, *J. Colloid Interf. Sci.*, 2008, **322**, 196.

24. J. Chen, X. Liu and F. Zhang, *Chem. Eng. J.*, 2015, **259**, 43.

25. E. Kok, N. Cant, D. Trimm and J. Scott, *Catal. Today*, 2011, **178**, 79.

26. J. W. Bae, Y.-J. Lee, J.-Y. Park and K.-W. Jun, *Energy Fuels*, 2008, **22**, 2885.

27. T. R. Jagannath, Dissertation (PhD), Saurashtra University, 2005.

28. Y.-J. Chen and C.-T. Yeh, *J. Catal.*, 2001, **200**, 59.

29. S. Y. Liu and S. M. Yang, *Appl. Catal. A: Gen.*, 2008, **334**, 92.

30. L. Delannoy, N. Weiher, N. Tsapatsaris, A. M. Beesley, L. Nchari, S. L.M. Schroeder and C. Louis, *Top. Catal.*, 2007, **44**, 263.

31. D. R. Lide, *Handbook of Chemistry and Physical Properties*, 88th edn., Taylor Francis, Boca Raton, 2007-2008.

32. F.-W. Chang, L. S. Roselin and T.-C. Ou, *Appl. Catal. A: Gen.*, 2008, **334**, 147.

33. Y. Pu, J. Zhang, X. Wang, H. Zhang, L. Yu, Y. Dong and W. Li, *Catal. Sci. Technol.*, 2014, **4**, 4426.

34. F. Cárdenas-Lizana, S. Gómez-Quero, H. Idriss and M. A. Keane, *J. Catal.*, 2009, **268**, 223.

35. A. Schulz and M. Hargittai, *Chem. Eur. J.*, 2001, **7**, 3657.

36. F. Cárdenas-Lizana, S. Gómez-Quero, N. Perret and M. A. Keane, *Catal. Sci. Technol.*, 2011, **1**, 652.

37. P. Claus, A. Brückner, C. Mohr and H. Hofmeister, *J. Am. Chem. Soc.*, 2000, **122**, 11430.

38. N. Lopez, J. K. Nørskov, T. V. W. Janssens, A. Carlsson, A. Puig-Molina, B. S. Clausen and J.-D. Grunwaldt, *J. Catal.*, 2004, **225**, 86.

39. P. V. Kamat, *J. Phys. Chem. C*, 2008, **112**, 18737.

40. D. Chen, J. Li, C. Shi, X. Du, N. Zhao, J. Sheng and S. Liu, *Chem. Mater.*, 2007, **19**, 3399.

41. S.-H. Zhou, Z. Ma, H.-F. Yin, Z.-L. Wu, B. Eichhorn, S. H. Overbury and S. Dai, *J. Phys. Chem. C*, 2009, **113**, 5758.

42. L. Deghedi, J.-M. Basset, G. Bergeret, J.-P. Candy, M. C. Valero, J.-A. Dalmon, A. de Mallmann, A.-C. Dubreuil and L. Fischer, in *10th International Symposium "Scientific Bases for the Preparation of Heterogeneous Catalysts"*, eds. E. M. Gaigneaux, M. Devillers, S. Hermans, P. Jacobs, J. Martens and P. Ruiz, Elsevier, Louvain-la-Newuve, 2010, vol. 175, p. 617.

43. A. M. Molenbroek and J. K. Nørskov, *J. Phys. Chem. B*, 2001, **105**, 5450.

44. T. P. Maniecki, K. Bawolak, D. Gebauer, P. Mierczynski and W. K. Jozwiak, *Kinet. Catal.*, 2009, **50**, 138.

45. W. C. Conner and J. L. Falconer, *Chem. Rev.*, 1995, **95**, 759.

46. J. Harris, *Surf. Sci.*, 1989, **221**, 335.

47. Z. Gu, L. Luo and M. Teng, *Indian J. Chem.*, 2007, **46A**, 742.

48. Y. X. Liu, J. X. Chen and J. Y. Zhang, *Chin. J. Chem. Eng.*, 2007, **15**, 63.

49. F. Cárdenas-Lizana and M. A. Keane, *J. Mat. Sci.*, 2013, **48**, 543.

50. R. Wojcieszak, S. Monteverdi, J. Ghanbaja and M. M. Bettahar, *J. Colloid Interf. Sci.*, 2008, **317**, 166.

51. J. Greeley and M. Mavrikakis, *Nature Mater.*, 2004, **3**, 810.

52. J. Greeley and M. Mavrikakis, *J. Phys. Chem. B*, 2005, **109**, 3460.

53. B. Pawelec, A. M. Venezia, V. La Parola, S. Thomas and J. L. G. Fierro, *Appl. Catal. A: Gen.*, 2005, **283**, 165.

54. X. Zhang, H. Shi and B.-Q. Xu, *Catal. Today*, 2007, **122**, 330.

55. T. V. Choudhary, C. Sivadinarayana, A. K. Datye, D. Kumar and D. W. Goodman, *Catal. Lett.*, 2003, **86**, 1.

56. Y. Azizi, C. Petit and V. Pitchon, *J. Catal.*, 2008, **256**, 338.

57. F. Cárdenas-Lizana, X. Wang, D. Lamey, M. Li, M. A. Keane and L. Kiwi-Minsker, *Chem. Eng. J.*, 2014, **255**, 695.

58. V. Vishwanathan, V. Jayasri, P. M. Basha, N. Mahata, L. M. Sikhwivhilu and N. J. Coville, *Catal. Commun.*, 2008, **9**, 453.

59. K. K. Yeong, A. Gavriilidis, R. Zapf and V. Hessel, *Catal. Today*, 2003, **81**, 641.

60. F. Cárdenas-Lizana, B. Bridier, C. C. K. Shin, J. Pérez-Ramírez and L. Kiwi-Minsker, *ChemCatChem*, 2012, **4**, 668.

61. H. Duan, D. Wang, Y. Kou and Y. Li, *Chem. Comm.*, 2013, **49**, 303.

62. P. Lu and N. Toshima, *Bull. Chem. Soc. Jpn.*, 2000, **73**, 751.

63. P. Lu, T. Teranishi, K. Asakura, M. Miyake and N. Toshima, *J. Phys. Chem. B*, 1999, **103**, 9673.

64. F. Cárdenas-Lizana, Z. Martínez de Pedro, S. Gómez-Quero and M. A. Keane, *J. Mol. Catal.*, 2010, **326**, 48.

65. C. Xiao, X. D. Wang, C. Lian, H. Q. Liu, M. H. Liang and Y. Wang, *Curr. Org. Chem.*, 2012, **16**, 280.

66. V. L. Khilnani and S. B. Chandalia, *Org. Proc. Res. Dev.*, 2001, **5**, 263.

67. K. Shimizu, Y. Miyamoto, T. Kawasaki, T. Tanji, Y. Tai and A. Satsuma, *J. Phys. Chem. C*, 2009, **113**, 17803.

68. E.-J. Shin and M. A. Keane, *J. Catal.*, 1998, **173**, 450.

69. W. W. Lonergan, D. G. Vlachos and J. G. Chen, *J. Catal.*, 2010, **271**, 239.

70. T. Wang, G. Mpourmpakis, W. W. Lonergan, D. G. Vlachos and J. G. Chen, *Phys. Chem. Chem. Phys.*, 2013, **15**, 12156.

Notes and references

Chemical Engineering, School of Engineering and Physical Sciences, Heriot-Watt University, Edinburgh, EH14 4AS, Scotland; Tel:+41(0)1314514719; E-mail:M.A.Keane@hw.ac.uk